MR1 Restricted Mucosal-Associated Invariant T (MAIT) Cells Respond to Mycobacterial Vaccination and Infection in Nonhuman Primates

Justin M. Greene[1,#], **Pradyot Dash**[2,1], **Sobhan Roy**[3,#], **Curtis McMurtrey**[4], **Walid Awad**[2], **Jason S. Reed**[1], **Katherine B. Hammond**[1], **Shaheed Abdulhaqq**[1], **Helen L. Wu**[1], **Benjamin J. Burwitz**[1], **Benjamin F. Roth**[1], **David W. Morrow**[1], **Julia C. Ford**[1], **Guangwu Xu**[1], **Joseph Y. Bae**[1], **Hugh Crank**[1], **Alfred W. Legasse**[1], **Thurston H. Dang**[5], **Hui Yee Greenaway**[5], **Monica Kurniawan**[5], **Marielle C. Gold**[6], **Melanie J. Harriff**[6,7], **Deborah A. Lewinsohn**[8], **Byung S. Park**[1], **Michael K. Axthelm**[1], **Jeffrey J. Stanton**[1], **Scott G. Hansen**[1], **Louis J. Picker**[1], **Vanessa Venturi**[9], **William Hildebrand**[4], **Paul G. Thomas**[2], **David M. Lewinsohn**[6], **Erin J. Adams**[3,10,*], and **Jonah B. Sacha**[1,*]

[*]Corresponding Authors: sacha@ohsu.edu; Phone: (503) 418-2774; Fax: (503) 418-2701, ejadams@uchicago.edu; Phone (773) 834-9816; Fax: (773) 702-0439.
[#]co-first authors

[1]Vaccine and Gene Therapy Institute and Oregon National Primate Research Center, Oregon Health & Science University, Beaverton, OR 97006, USA

[2]Department of Immunology, St. Jude Children's Research Hospital, Memphis, Tennessee 38105, USA

[3]Department of Biochemistry and Molecular Biology, University of Chicago, Chicago, IL 60637, USA

[4]Department of Microbiology and Immunology, University of Oklahoma Health Sciences Center, Oklahoma City, OK 73104, USA

[5]UNSW Australia, Sydney, New South Wales 2052, Australia

[6]Pulmonary & Critical Care Medicine, Oregon Health & Science University, Portland, OR 97239, USA

[7]VA Portland Health Care Services, Research & Development, 3710 SW US Veterans Hospital Rd, Portland, OR 97239 USA

[8]Molecular Microbiology and Immunology, Oregon Health & Science University, Portland, OR 97239, USA

[9]Kirby Institute for Infection and Immunity, UNSW Australia, Sydney, New South Wales 2052, Australia

[10]Committee on Immunology, University of Chicago, Chicago, IL 60637, USA

Abstract

Studies on mucosal-associated invariant T cells (MAITs) in nonhuman primates (NHP), a physiologically relevant model of human immunity, are handicapped due to a lack of macaque MAIT-specific reagents. Here we show that while MR1 ligand-contact residues are conserved between human and multiple NHP species, three T cell receptor (TCR) contact residue mutations in NHP MR1 diminish binding of human MR1 tetramers to macaque MAITs. Construction of naturally loaded macaque MR1 tetramers facilitated identification and characterization of macaque MR1-binding ligands and MAITs, both of which mirrored their human counterparts. Using the macaque MR1 tetramer we show that NHP MAITs activated *in vivo* in response to both BCG vaccination and *M. tuberculosis* infection. These results demonstrate that NHP and human MR1 and MAITs function analogously, and establish a preclinical animal model to test MAIT-targeted vaccines and therapeutics for human infectious and autoimmune disease.

Keywords

Introduction

Mucosal associated invariant T cells (MAITs) are non-classical T cells that-recognize microbial-derived vitamin B metabolites in the context of major histocompatibility complex (MHC) related protein 1 (MR1)[1,2]. MAITs comprise up to 10% of CD8+ T cells in the

peripheral blood of humans and accumulate in tissues like the liver, lung, and gut mucosa where these cells rapidly respond to microbial threats[3-5]. MAIT cells utilize a semi-invariant T cell receptor (TCR) to probe ligands bound by the highly conserved MR1 molecule. Like classical MHC class I molecules, MR1 is expressed by all nucleated cells, but its surface expression is often limited in the absence of appropriate ligand[6]. MAIT TCRs generally utilize a TRAV1-2 - TRAJ33 alpha chain combined with a more diverse array of beta chains, although novel MAIT cell populations utilizing other TCRs than TRAV1-2 have recently been identified[7,8]. Upon recognition of their cognate antigen, MAITs secrete inflammatory cytokines like IFNγ and TNFα. Moreover, MAITs are capable of this effector function immediately upon egress from the thymus[9]. Taken together, these features indicate that MAIT cells are an innate-like T cell subset primed to respond rapidly to bacterial pathogens.

Indeed, these innate like T cells play a role in the initial host response to *Mycobacterium tuberculosis* (Mtb) and other microbial pathogens including fungi and yeast[10-12]. MAITs have also been implicated in autoimmune diseases including multiple sclerosis and gut-associated diseases like colitis[13-16]. MAITs have been well characterized in mice and humans; however, their precise contribution to controlling and causing disease is unknown. In humans, MAITs are typically identified by expression of TCR vα7.2, CD161, and CD26. Nonhuman primates are a physiologically relevant model for studying infectious diseases like Mtb, but little is known about MAITs in these animals due to the lack of macaque-specific antibodies, MR1 tetramers, or a TCR repertoire analysis method[17,18].

Results

Nonhuman primate MR1 ligand identification

Mouse and human MR1-tetramers have facilitated the characterization of MAITs in each species[19,20]. Given that many human-specific reagents cross-react with the corresponding target on macaque cells, we were surprised to find that human MR1 tetramers folded with multiple ligands, as described below, exhibited a limited ability to stain rhesus macaque MAITs (see discussion of Fig. 1e below). To assess whether differences in the MR1 coding sequence might explain these results, we sequenced the functionally critical MR1 α1 and α2 domains from human, chimpanzee, rhesus macaque, cynomolgus macaque, Japanese macaque, pigtailed macaque, sooty mangabey, and baboon. Sequences were highly conserved among the different species, with greater than 95% nucleotide identity to human MR1 for all species examined (Supplemental Fig. 1). Despite this high level of sequence conservation, all nonhuman primate species, except chimpanzees, possessed three amino acid substitutions in previously-described MAIT TCR contact residues[21] (Fig. 1a,b). In contrast, sites known to form hydrogen bonds with the well-characterized MR1 ligand rRL-6-CH$_2$OH were conserved in every species[21]. These results suggested that the human MR1 tetramer might not effectively bind macaque MAITs due to variation at residues critical for TCR docking, but MR1 molecules from distinct primate species should bind and present identical ligands.

To test these hypotheses, we synthesized human and macaque MR1 tetramers using insect cells and the baculovirus expression system (Supplemental Fig. 2). The MR1 molecule was naturally loaded with ligand by infecting MR1-expressing Hi5 cells with *Escherichia coli* (*E.*

coli), and the secreted MR1 molecule subsequently purified via affinity chromatography. Because there is an array of potential ligands using this system, we hypothesized that we could use this monomer to identify the nearly full complement of putative MR1 ligands. Indeed, using liquid chromatography-mass spectrometry to identify macaque MR1 ligands as previously described, we identified approximately 40 putative MR1-ligands (data not shown)[22]. Although we are currently unable to assign structures to the majority of these ligands without confirmed spectra of the synthetic molecule, we identified the known activating ligand rRL-6-CH$_2$OH and a second ligand, 7-Hydroxy-6-methyl-8-ribityl lumazine (HMRL) (Fig. 1c,d). rRL-6-CH2OH and 5-OP-RU, both MAIT cell activating MR1 ligands, have the same chemical formula($C_{12}H_{18}N_4O7$) and are thus isoelemental. Additionally, these compounds have indistinguishable MS2 fragmentation spectra (PMID 23051753, 24695216, 24108697). Thus, it is possible that the compound identified here as rRL-6-CH2OH is 5-OP-RU or a mixture of both.

Nonhuman primate MR1 tetramers exhibit cross-reactive staining

We then used this newly synthesized human tetramer to stain PBMC samples from the same primate species used in our MR1 sequencing analysis above and found that the human tetramer was not universally cross-reactive and strictly stained human and chimpanzee MAITs (Fig. 1e). This staining pattern is consistent with the results from our MR1 sequencing in which human and chimpanzee MR1 sequences are identical at the previously noted TCR contact residues (Fig. 1a,b). In contrast to the results from the human MR1 tetramer, the macaque tetramer effectively stained MAITs from all eight species tested. The ability of macaque MR1 to stain human and chimpanzee MAITs is likely due to the amino acid substitutions at positions 72 and 151, residues which are known to mediate MR1 xenoreactivity[21,23] Although the anti-human Vα7.2 antibody exhibited variable cross-reactivity against nonhuman primate species, both macaque and human MR1 tetramer+ cells were Vα7.2+ in humans and chimpanzees confirming the tetramer specifically identifies MAITs (Fig. 1e; Supplemental Fig. 3a). Indeed, the human and macaque MR1 tetramer+ cells were also CD161+ in humans, although the anti-human CD161 antibody did not sufficiently cross-react with nonhuman primate CD161 to function as a marker in these species (Supplemental Fig. 3b). The unloaded macaque MR1-tetramer control did not stain cells from any species confirming that an appropriate ligand is required for the macaque MR1-TCR interaction (Fig. 1e). The MR1 tetramer staining in human samples mirrors previous studies in which MAITs are present in both the CD8+ and the CD8-CD4- populations; however, this double negative MAIT population was absent in every nonhuman primate species tested (Supplemental Fig. 3). These results provide the first demonstration of staining by a macaque MR1 tetramer and explain the limited cross reactivity observed with the human tetramer. Moreover, they demonstrate that the MR1 gene is highly conserved across several species but diverges at critical residues that affect TCR-MR1 docking. Finally, because this tetramer is loaded with a mixture of ligands, it is possible that it will identify additional MAIT populations that would be missed by a single ligand-loaded tetramer.

Functional and phenotypic characterization of nonhuman primate MAITs

Next, we sought to phenotypically and functionally characterize MR1 tetramer+ cells from rhesus macaques. In order to adapt the single-cell, unbiased TCRαβ analysis technique[24] to

macaques, we first extracted and characterized the TRA gene sequences from the rhesus macaque genome based on homology to the human TRA genes (Supplemental Fig. 4,5). Using this data and the TRB gene sequences we previously extracted from the rhesus macaque genome, we then performed paired sequencing of CDR3α and CDR3β from MR1 tetramer+ cells sorted from the liver and blood of a healthy macaque[25]. Consistent with results from humans, we found that the majority of MAITs utilized TRAV1-2 in conjunction with TRAJ33 (Fig. 2a)[20,26]. Additionally, most TCRα chains contained the canonical ligand-binding tyrosine (Fig. 2b and Supplemental Fig. 6)[27]. Previous studies of TCRα sequences across multiple species has demonstrated that these clonotypes can be efficiently produced by the gene recombination process due to 'overlap' between TRAV and TRAJ genes[28]. This means that the germline-encoded nucleotide sequences for these clonotypes can be produced by a variety of mechanisms. TRAV19 TCRα chains were also enriched in our sequence analysis (Supplemental Fig. 6). These TRAV19 sequences contained a common "NE" amino acid motif that may indicate shared recognition of the same MR1-ligand complex. This identification of TRAV1-2 negative MAITs is consistent with recent studies in humans[7,8]. The TCRα chains were relatively promiscuous in pairing with a variety of TCRβ chains (Supplemental Fig. 6a). Tetramer+ cells from the liver exhibited reduced diversity of TRAV and TRAJ usage compared to the blood MAITs (Fig. 2a). Additionally, there was liver-specific usage of TCRβ V regions suggesting tissue-specific differences in macaque MAITs parallel to previous results examining human MAIT TCRs[26] (Data not shown). These differences maybe be due, in part, to local clonal expansion or differential establishment of tissue residency, but will require additional in-depth study.

Previous studies examining human and mouse MAITs demonstrated that these cells express PLZF, a regulator of innate like T cell development, and RORγt, a master regulator of TH17 differentiation[7,19]. A proportion of MAITs have also been described as T-bet+, a marker associated with IFNγ production. We found that the majority of MR1 tetramer+ cells express PLZF and RORγt (Fig. 2d,e). MAITs expressed variable levels of T-bet that were indistinguishable from MR1 tetramer- CD8+ T cells, consistent with previous studies characterizing MAITs in mice and humans[19]. These data suggest that macaque MAITs might also produce higher levels of IFNγ compared to mice and further confirm that the macaque MR1 tetramer is identifying macaque MAITs. Finally, we assessed MR1 tetramer+ cell function in an *E. coli*-based stimulation assay[3]. MAIT activation is MR1 dependent, and should not be blocked by the pan-MHC-I blocking antibody W6/32[29]. MR1 tetramer+ cells produced significant amounts of IFNγ and TNFα, and upregulated CD69 in response to *E. coli* (Fig. 2f,g). This activation was reduced by MR1 blockade, but not by the isotype control or pan-MHC-I blocking antibody (Fig. 2f). In contrast, MR1 tetramer- CD8+ cells produced very little IFNγ and/or TNFα in response to *E. coli* stimulation and this was not significantly reduced by anti-MR1 antibody (Fig. 2g). Interestingly, MAITs did not produce significant amounts of IL-17 in these assays (data not shown). These results demonstrate that macaque MR1 tetramer specifically stains macaque MAITs and macaque MAITs are activated in response to bacteria in an MR1-dependent fashion.

Next, we assessed the distribution and phenotype of MAITs across 23 different tissues in 11 Indian rhesus macaques. We found that MAITs were most abundant in the epithelium of the lung (measured by bronchoalveolar lavage, BAL) and in liver (Fig. 3a,b). We did not detect

high frequencies of MAITs in lymph nodes or other primary and secondary lymphoid organs. We also examined MAIT activation by Ki-67 and CD69 staining, and observed nearly equivalent frequencies of Ki-67+ MAITs and non-MAIT CD8+ T cells in most tissues (Fig. 3c). We focused our statistical analysis on BAL, liver, and blood, and found small differences in Ki-67 expression in BAL and liver compared to non-MAIT CD8+ T cells. In contrast, MAITs expressed higher levels of CD69 than non-MAITs in most primary lymphoid tissues, secondary lymphoid tissues, and select extralymphoid tissues (Fig. 3d). We observed significantly more CD69+ MAITs than non-MAIT CD8+ T cells in the liver while these frequencies were essentially equivalent in the blood and BAL. These results suggest that MAITs may actively encounter and respond to bacterial antigens in the liver, particularly as the liver filters blood from the intestinal tract[30]. We also examined the memory phenotype of MAITs in these tissues and found that the majority of MAITs were CD28+CD95+ memory T cells (Supplemental Fig. 7a). Further analysis revealed that MAITs in the primary and secondary lymphoid tissues, particularly the lymph nodes, exhibited a mostly central memory (CCR7+, CD28+) phenotype while in extralymphoid tissues they exhibited a transitional effector memory (CCR7-, CD28+) or effector memory (CCR7-, CD28-) phenotype (Supplemental Fig. 7b). Human blood MAITs are traditionally considered effector memory T cells as defined by CD45RA and CD62L expression[31]. While T cell memory markers differ between the two species, we find that macaque MAITs exhibit a spectrum of memory phenotypes largely dependent on their anatomical location. It is currently unclear why a higher frequency of macaque MAITs exhibit a central memory phenotype compared to human MAITs. These results highlight the differences in MAITs among distinct tissues, possibly reflecting differences in antigen exposure at these sites.

MAITs respond to mycobacterial infection in vivo

We next utilized the macaque model to examine the functional response of MAITs to bacterial challenge *in vivo*. Following intradermal vaccination with Bacillus Calmette-Guerin (BCG) to the left and right chest of each animal, we failed to observe a significant and consistent change in MAIT frequency in peripheral blood (Fig. 4a). In contrast, MAITs became specifically activated in response to BCG vaccination in the blood at days 14 and 21 post-vaccination compared to baseline while non-MAIT CD8+ T cells did not (Fig. 4b). Nine weeks after the initial BCG vaccination, we re-vaccinated the macaques, and two weeks later collected skin from the sites of vaccination on the chest (pectoral) and skin from the inner thighs (inguinal) as a non-vaccination control site, as well as spleen, blood, BAL, axillary lymph node, and inguinal lymph node. While not significant, we observed a trend toward higher frequencies of MAITs in skin at the site of vaccination compared to skin from a distal site (Fig. 4c,d). Further, we measured significantly higher frequencies of Ki-67+ MAITs in the vaccine site compared to the distal inguinal skin (Fig. 4e). Moreover, MAITs from the vaccine site were also significantly more activated than non-MAIT CD8+ T cells from the same site (Fig. 4g). In contrast, non-MAIT CD8+ T cells tended to be more activated in the distal inguinal skin (Fig. 4g). Measurements of activated MAITs in the draining axillary lymph nodes compared to the distal inguinal lymph nodes mirrored those in the vaccination site skin and distal skin (Fig. 4e,g). While contemporaneous uninfected controls were not available, the Ki-67 expression in MAITs from axillary lymph nodes of BCG infected macaques was nearly 10-fold higher than MAITs from axillary lymph nodes

of healthy, non-vaccinated animals (Fig. 3c, 4e). Finally, we also found a higher frequency of granzyme B-loaded MAITs in skin at the vaccination site and the draining axillary lymph node compared to the distal skin and lymph nodes (Fig. 4f), demonstrating that BCG vaccination licenses MAITs via granzyme B[3]. Longitudinal analysis after the revaccination showed that, while not significant, blood. MAITs were activated again at day 14 post-vaccination (Fig. 4h). These results demonstrate that MAITs are specifically activated in response to bacterial threats in the nonhuman primate. Additionally, these data demonstrate the need to examine MAIT cells in the relevant tissues because measurements from blood alone may miss MAIT cell activation, and further reveal the unique advantages of the nonhuman primate model, where longitudinal tissue biopsies may be taken.

Finally, we examined the MAIT response to Mtb infection. We monitored nine intrabronchially Mtb-infected macaques for eight weeks post challenge for changes in MAIT frequency and activation in blood. Similar to BCG vaccination, we did not observe a consistent change in MAIT frequencies in peripheral blood (Fig. 4i). It is possible that MAITs expanded locally in the lung in response to infection and that measurements in the blood missed this local expansion. We again observed an increase in Ki-67+ MAITs in the blood over the course of infection; however, we observed a similar increase in activated non-MAIT CD8+ T cells as well (Fig. 4j). The activation of non-MAIT CD8+ T cells is consistent with the higher pathogenicity of Mtb infection compared to BCG vaccination[32]. These results further illustrate that macaque MAITs are activated and respond rapidly to bacterial infection. Future studies examining lung MAITs in Mtb infection may reveal more rapid activation compared to blood MAIT responses.

Discussion

Here, we thoroughly characterized nonhuman primate MAITs and demonstrated their capacity to respond to bacterial threats. We utilized a novel strategy to synthesize macaque and human MR1 molecules that bind a wide breadth of different ligands. Elution studies from these naturally loaded MR1 molecules revealed a surprising spectrum of previously unidentified ligands, which will serve to further our understanding of MR1 function. Importantly, however, we found that MR1 molecules from different primate species bind identical ligands. This conservation indicates an important role for MAIT cells in the primate immune response, and suggests that studies of MR1 in macaques are directly applicable to human MR1. When the naturally loaded MR1 molecule is used as a tetramer reagent, it likely stains a greater diversity of MAIT cells as indicated by the variety of TCRs we identified. While the TRAV1-2 and TRAJ33 were common among the MAIT cells we sequenced, we also identified additional, non-canonical TCRs (TRAV19) that a single-ligand tetramer might not bind.

In addition to establishing MR1 and MAIT function in macaques, we have annotated the rhesus macaque TCRα genes in order to perform single cell paired TCRαβ analysis. This technique will now facilitate a more detailed investigation of the TCR repertoire in macaque studies of ageing, host defense, and autoimmunity, thereby increasing the utility of this animal model. Indeed, paired with the macaque MR1 tetramer, this technique can now

inform us how the MAIT TCR repertoire changes in response to vaccination and infection, and whether tissue- or pathogen-specific MAIT TCR signatures exist.

MAITs are an important component of host immunity to Mtb infection, and represent a potential new vaccine target. Using the MR1 tetramer made here, future macaque studies can directly examine if MAITs play a role in controlling Mtb or other bacterial infections, and test whether their function, phenotype, and anatomical distribution can be modulated through the rational design of novel vaccine immunogens. While we did not observe MAIT cell expansion in the blood of Mtb infected macaques, we hypothesize that expansion occurred at the site of infection in the lung. Unfortunately, we were unable to specifically measure lung immunity in the current study. However, given the ability to perform repeated longitudinal lung biopsies or BAL in macaques, future Mtb studies in macaques can definitively investigate pulmonary MAIT immunity. Ultimately, this study demonstrates the power of the nonhuman primate model to interrogate MAIT biology and provides a foundation for studying the role of MAITs in both infectious disease and autoimmune disorders.

Methods

Live subjects and bacteria

Seventeen nonhuman primates were followed longitudinally in this study. All animals were cared for at the Oregon National Primate Research Center (ONPRC) with the approval of the ONPRC Animal Care and Use Committee using the standards of the NIH Guide for the Care and Use of Laboratory Animals. Four Indian rhesus macaques were challenged intradermally with 2×10^5 live units of BCG Vaccine SSI. Half of the dose was delivered to the left and right chest of each animal. Nine rhesus macaques were infected intrabronchially with 10 CFU of *Mycobacterium tuberculosis* Erdmann strain. Details on the clinical progression of the animals can be found in Hansen SG *et al.* (manuscript in preparation). Cyropreserved or fresh samples from an additional 43 nonhuman primates were used in this study, which were assigned to other, unrelated studies. Cyropreserved samples were used in the cross species stain, TCR sequencing experiments, and functional assay. We observed no loss of function by cryopreserved splenocytes compared to fresh PBMCs (data not shown).

Expression of soluble macaque MR1 protein, ligand loading and biotinylation for tetramer preparation

Macaca mulatta MR1 and β_2m genes were expressed as a single chain construct in insect cells using the baculovirus expression system (Supplemental Fig. 2a,b). The β_2m gene was fused with the ectodomain of MR1 gene with a flexible glycine serine linker. The BirA biotinylation sequence (avitag), 3C protease digestion sequence and 6X histidine tag were added at the C-terminal end of MR1 and cloned into the pACGP67A vector (BD biosciences) downstream of the gp67 secretion signal sequence. A second construct was made only with a 6X histidine tag at the C-terminal end (Supplemental Fig. 2a). Baculovirus containing MR1 constructs were generated following the transfection and amplification in Sf9 cells. MR1 was loaded with *E. coli* ligands following a co-infection method during MR1 expression in Hi5 cells. Specifically, Hi5 cells were grown in antibiotic free media and

infected with MR1 containing baculovirus. After 18 -20 hrs of incubation, Hi5 cells were co-infected with *E. coli* strain BL21 (40 cells/ml) from an overnight culture. Hi5 cells were harvested after 65 - 68 hrs and supernatant containing the secreted MR1 was collected by centrifugation. The pH of the supernatant was adjusted to 7.2 with HEPES or Tris (Fisher scientific) buffer and buffer exchanged with HEPES buffered saline (HBS: 10 mM HEPES, pH-7.2, 150 mM NaCl and 0.02% azide). MR1 proteins were purified from supernatant using Ni-NTA affinity chromatography (Qiagen). Ni-NTA agarose and imidazole (final concentration of 20 mM) were added to the supernatant and incubated overnight on a rotator. The next day, protein was eluted with HBS and 200 mM imidazole, and fractions were checked on SDS-PAGE. MR1 containing fractions were pooled, buffer exchanged to HBS with 20 mM imidazole and treated with 3C protease overnight at 4°C to remove the histidine tag. Protein was again passed through the Ni-NTA column to remove contaminants and flow through was collected. MR1 was buffer exchanged three times with 20 mM Tris pH-8.0, 50 mM NaCl and concentrated. MR1 was biotinylated using the BirA enzyme in presence of buffer-A (50 mM bicine buffer, pH 8.3) and buffer-B (10 mM ATP, 10 mM MgOAc and 50 μM d-biotin) (Avidity, LLC). After 5 hrs of incubation at room temperature MR1 was purified using S200 size exclusion chromatography (GE healthcare) and checked for biotinylation in non-reducing SDS-PAGE with streptavidin (Supplemental Fig. 2c). For ligand identification experiments, MR1 histidine tagged protein was loaded similarly with *E. coli* ligands, purified with Ni-NTA and S200 size exclusion chromatography.

Sequencing and sequence analysis

DNA and RNA were isolated from approximately 3×10^6 PBMCs from all primate species using the Qiagen DNA/RNA Allprep Kit. cDNA was then synthesized using the SuperScript III Reverse Transcriptase (ThermoFisher Scientific). Amplicons of MR1 sequences were generated via amplification of cDNA by PCR using high-fidelity Phusion™ polymerase (New England Biolabs) and the primers below with the following thermocycling conditions: 50°C for 30min, (94°C for 15s, 55°C for 1m, 68°C for 1m) for 35 cycles, and 68°C for 5min. The forward primers used were as follows: Human – 5′-ATGGCGTTCCTGTTACCTC-3′, Chimpanzee – 5′-ATGGGGGAACTGATGGCG-3′, and all others – 5′-ATGGTGTTCTTGTTACCTCTC-3′. The sequence of the reverse primer was 5′-TCATCGATCTGGTGTCGG-3′. Sequencing was performed at the ONPRC Genetics Core by Sanger's sequencing using the above primers. Analysis of the sequences was performed using CodonCode Aligner (CodonCode Corporation) and Geneious-Pro software (Biomatters Ltd.).

LCMS analysis of Macaque MR1

Approximately 5μg of macaque MR1 expressed in the presence of *E. coli* or media only was injected for low pH reverse-phase nano-scale LCMS. Nano-LCMS was performed using an Eksigent nano-LC-4000 with an Eksigent autosampler (Sciex). Mobile phase solvents were: solvent A (98% water, 2% acetonitrile, 0.1% formic acid), and solvent B (95% acetonitrile, 5% water, 0.1% formic acid). Whole MR1 was loaded onto a C18 trap column (350 μm [i.d.] × 0.5 mm long; ChromXP) and desalted at 5μl/min for 5 minutes using 100% solvent A. After desalting, the trap was placed in line with a C18 separation column (75 μm [i.d.] × 15 cm long; ChromXP). Sample was then eluted at 300 nl/min using two linear gradients: 1. 5%

solvent B to 35% solvent B in 15 minutes, 2. 35% solvent B to 60% solvent B. Eluate was ionized using a Nanospray III ion source (Sciex). Ion spectra were collected using an AB Sciex TripleTOF 5600 mass spectrometer. Data was acquired in data-dependent acquisition mode with a m/z range of 150-1500 in negative ion polarity. Extracted ion chromatograms, MS1 survey spectra, and MS2 fragment spectra were made using PeakVeiw 1.2 (Sciex).

Cell processing

PBMC was isolated from EDTA-treated whole blood using Ficoll-Paque (GE Healthcare) density-centrifugation as previously described[33]. Cells were resuspended in RPMI 1640 containing 10% FBS (R10, Hyclone Laboratories). All other tissues except for lung, liver, colon, and skin were prepared into single-cell suspensions by dicing in a large petri dish and then pressing over a 70μM cell strainer. Colon was first diced and then rinsed with R3 containing 0.1M DTT (Promega) and shaken at 225rpm in a shaker incubator for 10 minutes at 37°C. Next the DTT media was aspirated and the colon pieces were shaken for 45 minutes in R3 media with 5ml of 0.5M EDTA. Colon pieces were then poured over a tea strainer and rinsed thoroughly with HBSS. Colon pieces were then shaken for one hour at 225rpm in R3 containing 0.1mg/ml collagenase (Sigma-Aldrich) and 0.1mg/ml DNase (Roche). After one hour, colon pieces were pressed over a 70um cell strainer and rinsed thoroughly with HBSS. 500ul of 0.5M EDTA was added to stop collagenase activity. Colon cells were pelleted and then resuspended in approximately 40ml of isotonic percoll (GE Biosciences) diluted to 70% with R3. This cell suspension was then underlayed below 7ml of isotonic percoll diluted to 37% with 1×PBS in 8 tubes and spun at 550g for 20 minute with no brake and acceleration minimized. After spinning, cells at the interface were removed using a transfer pipet and placed in R10. Cells were centrifuged at 830g for 4 minutes and then resuspended in an appropriate volume for counting. Liver was treated in EDTA, digested, and underlayed in percoll as described above. Lung and skin were diced, digested and centrifuged in percoll as described above.

Cell staining

Approximately 1-2×10^6 cells were placed in 50-100ul of R10 media for tetramer staining purposes, with or without 50nM dasatinib[34]. Tetramer was added at a final concentration of 100nM and cells were incubated in the dark at room temperature for one hour. Surface staining antibodies were then added and cells were incubated for an additional 30 minutes in the dark at room temperature. Cells were then washed once with 1×PBS and fixed with 2% PFA for surface stains or the fix/perm reagent from the eBioscience Foxp3 / Transcription Factor Staining Kit. Antibodies used in this study included: anti-CD3 (clone: SP34-2, Pacific Blue, BD Biosciences), anti-CD3 (clone: CD3-1, unconjugated, Mabtech), anti-CD8 (clone: SK1, TruRed, BD Biosciences), anti-CD4 (clone: L200, PE-Cy7, BD Biosciences), anti-CD28 (clone: CD28.2, PE, BD Biosciences), anti-CD95 (clone: DX2, FITC, BD Biosciences), anti-CD69 (clone: FN50, ECD, Biolegend), anti-CCR7 (clone: 150503, Pacific Blue, R&D Systems), anti-IFNγ (clone: B27, FITC, BD Biosciences), anti-TNF (clone: MAb11, Alexa 700, BD Biosciences), anti-IL-17A (clone: eBio64DEC17), anti-PLZF (clone: Mags.21F7, PE, eBioscience), anti-RORγ(t) (clone: AFKJS-9, PE, eBioscience), anti-T-bet (clone: 4B10, PE-Cy7, eBioscience) Vα7.2 (clone: 3C10, APC-Cy7, Biolegend), CD161 (clone: 3G10, FITC, Biolegend). LIVE/DEAD Fixable Yellow Dead Cell Stain (Life

Technologies) was used to assess cell viability. Intracellular stains used the Foxp3 / Transcription Factor Staining Kit. Stains were run on the LSR II (BD Biosciences) and then analyzed using FlowJo, Version 10.0.8 or 9.9 (TreeStar).

Design of TCR segment-specific primers

To design a nested multiplex PCR approach to analyze the paired TCRαβ repertoire at the single cell level in macaque, we adapted a similar strategy to that described for mouse and human single cell PCR for TCR repertoire analysis[24,35,36]. Unlike mouse and human, an annotated *TCRa/d* locus was not available for macaque in any database. It has been reported that the humans and chimpanzees share 98.6% identity of their genomes and a previous comparative analysis of the TCRβ chain of rhesus macaques and humans reported that their TCRβ chains are highly similar (92.9%) at the nucleotide level[25,37]. With this knowledge we first assessed the cross-priming of published individual human TRAV and TRBV forward primers with their corresponding reverse primers (TRAC and TRBC reverse primers) using the total RNA harvested from macaque CD8+ T cells[24,36]. As shown in Supplemental Fig. 8, the majority (96.55%) of the macaque TRBV families were amplified by the human external and internal set of forward primers. However, only 35% of the macaque TRAV families showed amplification by the published human TRAV external and internal primers (data not shown). Therefore we downloaded the macaque *tcra/d* locus from NCBI and redesigned the mismatched TRAV primers in a species-specific manner. The TCRα chain constant region sequence was extracted based on the sequence information published and the reverse external and internal primers were designed using CLCbio software (Qiagen)[38]. A total of 37 (TRAV) and 29 (TRBV) external/internal pairs of sense primers and a pair of antisense primers (external/internal for the TRAC and TRBC genes were synthesized at standard desalted purity (IDT). The macaque-specific TRAV primer panel consisting of newly designed macaque specific and cross-priming human TRAV primers were validated as before (Supplementary Fig. 8)[36]. The complete list of primers is shown in Supplemental Figure 9.

Single cell sorting

PBMCs and the lymphocytes from the liver biopsy were resuspended at 2×10^7 per ml of PBS. 3×10^6 cells were stained with Fixable Live/Dead Aqua (Molecular Probes) in 200μl volume for 20 minutes at room temperature in the dark. The cells were centrifuged and the cell pellet was resuspended in 150μl of sort buffer (PBS containing 0.1% BSA, Fraction V (Gibco)) containing 100nM MR1-APC tetramer. The cells were incubated with the tetramer for 1 hr at room temperature in the dark. Following incubation, an antibody master mix consisting of CD3-PacBlue and CD8-PerCPCy5.5 in sort buffer was added to the tubes and pulsed by vortexing 2-3 times. The cells were further incubated on ice for 30 minutes in dark. After the incubation, the cells were washed twice with sort buffer by centrifuging at 500g for 5 minutes. The cell pellet was resuspended in sort buffer (containing 200 units of RNAsin/ml (Promega)) and filtered through 40μM cell strainer prior to sorting. The MR1-tetramer+CD8+CD3+ T cells were single cell sorted into the wells of a 96-well PCR plate (Eppendorf) using a iCyt Synergy cell sorter (Sony) with following settings: Multi-drop sort OFF, Multi-drop exclude OFF, Division 10, Center sort%: 90. The last two columns of the plate (11 and 12) were left unsorted to use as negative controls for the PCR. After sorting,

the plates were sealed using plate sealer film (MicroAmp, Applied Biosystems) and centrifuged at 500g for 3 minutes and stored at -80°C until reverse transcription and PCR.

TCR RT-PCR and sequencing

The cDNA synthesis was performed directly from single cells without any RNA extraction step using the SuperScript VILO cDNA synthesis kit (Thermo Scientific) with minor modification of the manufacturer's instructions. The cDNA synthesis was carried out in 2.5 μl of reaction mix comprising of 0.5 μl of 5X VILO reaction mix, 0.25 μl of 10X SuperScript® Enzyme mix, 0.25μl of 1% Triton X-100 (Sigma). The reaction was performed by using the following program in a thermocycler: 25°C for 10 min, 42°C for 60 min, and 85°C for 5 min. Following reverse transcription, a multiplex nested PCR was carried out using a Taq polymerase based PCR kit (Qiagen). The PCR reaction recipe for first and second round PCR were performed as previously described except for the primer components[24,36,39]. For the first-round PCR, a cocktail of TRAV and TRBV specific forward primers (each primer at 0.1 μM final concentration) and both TRAC and TRBC specific anti-sense primers (0.2 μM final concentration) was used (Supplementary Fig. 9). For the nested PCR, the reaction for the TCRα chains and TCRβ chains were setup separately using 2.5 μl of the first-round PCR products to serve as templates. The PCR mix for TCRα and TCRβ consisted of the same recipe as described with corresponding internal sense TRAV primers and internal antisense TRAC primer or internal sense TRBV primers and internal antisense TRBC primer, respectively (Supplementary Fig 8)[24,36]. The PCR conditions were 95°C for 5 min, followed by 34 cycles of 95°C for 20s, 52°C for 20s, and 72°C for 45s, followed by a final extension of 72°C for 7 min. At the end of the PCR cycle, the PCR products were visualized on 2% agarose gel (Supplementary Fig. 10). The PCR products were purified by Exonuclease I/Shrimp Alkaline Phosphatase treatment and sequenced as described with the relevant TRAC or TRBC internal primer using a ABI Big Dye sequencer (Applied Biosystem) at the Hartwell Center, St Jude Children's Research Hospital[24]. The sequence data was analyzed using a custom-built macro-enabled Microosft Excel sheet and IMGT to derive CDR3 nucleotide and amino acid sequences. To determine the corresponding TRAV-TRAJ or TRBV/TRBJ usage, the sequence data derived from single cells was compared with the extracted macaque specific TRAV/TRAJ and the downloaded TRBV/TRBJ genes (from IMGT) by using the BLAST algorithm locally (CLCbio, Qiagen).

Extraction of the TRAV, TRDV, and TRAJ genes from the rhesus macaque genome

The published rhesus macaque (*Macaca mulatta*) genome is available from the National Center for Biotechnology Information (NCBI) Rhesus Macaque Genome Resources website (http://www.ncbi.nlm.nih.gov/projects/genome/guide/rhesus_macaque/)[40]. The TRA and TRD gene locus are located on chromosome 7 (Accession number: NC_007864.1). The human TR reference genes (i.e. *01 alleles) were obtained from the IMGT/GENEDB database (downloaded on 9 December 2010)[41]. To extract the TRA and TRD genes from the rhesus macaque genome we used a method similar to the one we previously used to extract the TRB genes from the rhesus macaque genome[25]. The rhesus macaque chromosome 7 sequence was queried against all human TRA and TRD reference gene sequences using BLAST (Basic Local Alignment Search Tool, version 2.2.20) to identify regions in the

rhesus macaque sequence that resembled the human TR genes[42]. Results were filtered to those with e-value 0.001, a match to 35% of the query human reference gene, and total percent identity 75% with the human reference gene. Overlapping regions from the BLAST searches against all TR genes were then merged and the resultant regions were extended by 300 base pairs in both the 5′ and 3′ directions to account for regions that may have been missed due to the BLAST local alignment. These regions of the rhesus macaque genome were then compared against each of the human TR reference genes using EMBOSS Needle 6.0.0 (gap open: 10, gap extend: 4), which uses the Needleman-Wunsch algorithm[43]. These global alignments were used to identify the best human match to each region of the rhesus macaque genome, to determine the terminal ends of the rhesus macaque gene sequences, and to determine the various gene regions (i.e. intron, exon, and recombination signal sequences). TRA and TRD sequences available from the Dryad Digital Repository: http://dx.doi.org/10.5061/dryad.vm36c.

MAIT ICS

A small seed culture of DH5α *E. coli* was inoculated and incubated on a shaker at 37°C overnight. The following day, a 1:50 – 1:100 dilution was prepared and shaken until it reached approximately 5×10^8 cells/ml as estimated by OD600 on a spectrophotometer. The *E. coli* were then fixed using 2% PFA for 20 minutes. The *E. coli* were then washed and resuspended in complete media for addition to the assay at a 15:1 bacteria to cell ratio. PBMC or splenocytes were resuspended at 2×10^7 cells/ml and 50ul (1×10^6) cells were added to each well of a 96 well round bottom plate in R10. Blocking antibodies were added one hour prior to the addition of *E. coli* at a concentration of 100ug/ml and cells were incubated at 37°C and 5% CO_2 for one hour. After the addition of *E. coli*, cells were incubated for another hour before the addition of Brefeldin A (Sigma Aldrich) and co-stimulatory molecules CD28 and CD49d (BD Biosciences). Cells were incubated for 8 hours at 37°C and 5% CO_2, then refrigerated until the following day. Cells were washed 5 times to remove blocking antibodies and stained with tetramer and surface staining antibodies. Then intracellular stains were performed using the eBioscience Foxp3 / Transcription Factor Staining Buffer Set.

Statistical analysis

Due to small sample sizes, we could not assess the normality of our data and utilized non-parametric tests throughout our analysis. For tissue MAIT frequency and functional assay analysis, we used the Kruskal Wallis test to evaluate differences between each column, and pre-planned contrasts test using Dunn's test was performed to correct the overall type I error rate. We used the Wilcoxon Rank Sum test to compare Ki-67 and CD69 frequencies in select tissues. We used the Friedman Test in the longitudinal BCG and TB study to detect differences between time points. When significant, we used Dunn's Multiple Comparison post-test to compare each time point to day 0.

Supplementary Material

Refer to Web version on PubMed Central for supplementary material.

Acknowledgments

Literature Cited

1. Napier RJ, Adams EJ, Gold MC, Lewinsohn DM. The Role of Mucosal Associated Invariant T Cells in Antimicrobial Immunity. Front Immunol. 2015; 6:344. [PubMed: 26217338]

2. Kjer-Nielsen L, et al. MR1 presents microbial vitamin B metabolites to MAIT cells. Nature. 2012; 491:717–723. [PubMed: 23051753]

3. Kurioka A, et al. MAIT cells are licensed through granzyme exchange to kill bacterially sensitized targets. Mucosal Immunol. 2015; 8:429–440. [PubMed: 25269706]

4. Le Bourhis L, et al. MAIT cells detect and efficiently lyse bacterially-infected epithelial cells. PLoS Pathog. 2013; 9:e1003681. [PubMed: 24130485]

5. Le Bourhis L, et al. Antimicrobial activity of mucosal-associated invariant T cells. Nat Immunol. 2010; 11:701–708. [PubMed: 20581831]

6. Harriff MJ, et al. Endosomal MR1 Trafficking Plays a Key Role in Presentation of Mycobacterium tuberculosis Ligands to MAIT Cells. PLoS Pathog. 2016; 12:e1005524. [PubMed: 27031111]

7. Gherardin NA, et al. Diversity of T Cells Restricted by the MHC Class I-Related Molecule MR1 Facilitates Differential Antigen Recognition. Immunity. 2016; 44:32–45. [PubMed: 26795251]

8. Meermeier EW, et al. Human TRAV1-2-negative MR1-restricted T cells detect S. pyogenes and alternatives to MAIT riboflavin-based antigens. Nat Comms. 2016; 7:12506.

9. Gold MC, et al. Human thymic MR1-restricted MAIT cells are innate pathogen-reactive effectors that adapt following thymic egress. Mucosal Immunol. 2013; 6:35–44. [PubMed: 22692454]

10. Gold MC, et al. Human mucosal associated invariant T cells detect bacterially infected cells. PLoS Biol. 2010; 8:e1000407. [PubMed: 20613858]

11. Sharma PK, et al. High expression of CD26 accurately identifies human bacteria-reactive MR1-restricted MAIT cells. Immunology. 2015; 145:443–453. [PubMed: 25752900]

12. Chua WJ, et al. Polyclonal mucosa-associated invariant T cells have unique innate functions in bacterial infection. Infect Immun. 2012; 80:3256–3267. [PubMed: 22778103]

13. Serriari NE, et al. Innate mucosal-associated invariant T (MAIT) cells are activated in inflammatory bowel diseases. Clin Exp Immunol. 2014; 176:266–274. [PubMed: 24450998]

14. Haga K, et al. MAIT cells are activated and accumulated in the inflamed mucosa of ulcerative colitis. J Gastroenterol Hepatol. 2015; :n/a–n/a. DOI: 10.1111/jgh.13242

15. Willing A, et al. CD8$^+$ MAIT cells infiltrate into the CNS and alterations in their blood frequencies correlate with IL-18 serum levels in multiple sclerosis. Eur J Immunol. 2014; 44:3119–3128. [PubMed: 25043505]

16. Held K, et al. αβ T-cell receptors from multiple sclerosis brain lesions show MAIT cell-related features. Neurol Neuroimmunol Neuroinflamm. 2015; 2:e107–e107. [PubMed: 25977934]

17. Vinton C, et al. MAIT cells are systemically depleted in SIV-infected rhesus macaques. J Virol. 2016; JVI.02876–15. doi: 10.1128/JVI.02876-15

18. De Rose R, Fernandez CS, Hedger MP, Kent SJ, Winnall WR. Characterisation of macaque testicular leucocyte populations and T-lymphocyte immunity. J Reprod Immunol. 2013; 100:146–156. [PubMed: 24139314]

19. Rahimpour A, et al. Identification of phenotypically and functionally heterogeneous mouse mucosal-associated invariant T cells using MR1 tetramers. J Exp Med. 2015; 212:1095–1108. [PubMed: 26101265]

20. Reantragoon R, et al. Antigen-loaded MR1 tetramers define T cell receptor heterogeneity in mucosal-associated invariant T cells. J Exp Med. 2013; 210:2305–2320. [PubMed: 24101382]

21. López-Sagaseta J, et al. The molecular basis for Mucosal-Associated Invariant T cell recognition of MR1 proteins. Proc Natl Acad Sci U S A. 2013; 110:E1771–8. [PubMed: 23613577]

22. Yaciuk JC, et al. Direct interrogation of viral peptides presented by the class I HLA of HIV-infected T cells. J Virol. 2014; 88:12992–13004. [PubMed: 25165114]

23. Huang S, et al. MR1 antigen presentation to mucosal-associated invariant T cells was highly conserved in evolution. Proc Natl Acad Sci U S A. 2009; 106:8290–8295. [PubMed: 19416870]

24. Dash P, Wang GC, Thomas PG. Single-Cell Analysis of T-Cell Receptor αβ Repertoire. Methods Mol Biol. 2015; 1343:181–197. [PubMed: 26420718]

25. Greenaway HY, et al. Extraction and characterization of the rhesus macaque T-cell receptor beta-chain genes. Immunology and Cell Biology. 2009; 87:546–553. [PubMed: 19506572]

26. Lepore M, et al. Parallel T-cell cloning and deep sequencing of human MAIT cells reveal stable oligoclonal TCRβ repertoire. Nat Comms. 2014; 5:3866.

27. Reantragoon R, et al. Structural insight into MR1-mediated recognition of the mucosal associated invariant T cell receptor. J Exp Med. 2012; 209:761–774. [PubMed: 22412157]

28. Greenaway HY, et al. NKT and MAIT invariant TCRα sequences can be produced efficiently by VJ gene recombination. Immunobiology. 2013; 218:213–224. [PubMed: 22647874]

29. Gold MC, et al. Human innate Mycobacterium tuberculosis-reactive alphabetaTCR+ thymocytes. PLoS Pathog. 2008; 4:e39. [PubMed: 18282101]

30. Jeffery HC, et al. Bacteria Exposed Biliary Epithelium and Liver B Cells Activate Intrahepatic Mait Cells in an MR1-Dependent Manner. J Hepatol. 2015; doi: 10.1016/j.jhep.2015.12.017

31. Fergusson JR, et al. CD161 defines a transcriptional and functional phenotype across distinct human T cell lineages. Cell Rep. 2014; 9:1075–1088. [PubMed: 25437561]

32. Ryan AA, et al. Antigen Load Governs the Differential Priming of CD8 T Cells in Response to the Bacille Calmette Guerin Vaccine or Mycobacterium tuberculosis Infection. J Immunol. 2009; 182:7172–7177. [PubMed: 19454714]

33. Burwitz BJ, et al. CD8+ and CD4+ cytotoxic T cell escape mutations precede breakthrough SIVmac239 viremia in an elite controller. Retrovirology. 2012; 9:91. [PubMed: 23131037]

34. Lissina A, et al. Protein kinase inhibitors substantially improve the physical detection of T-cells with peptide-MHC tetramers. J Immunol Methods. 2009; 340:11–24. [PubMed: 18929568]

35. Dash P, et al. Paired analysis of TCRα and TCRβ chains at the single-cell level in mice. J Clin Invest. 2011; 121:288–295. [PubMed: 21135507]

36. Wang GC, Dash P, McCullers JA, Doherty PC, Thomas P. G. T cell receptor αβ diversity inversely correlates with pathogen-specific antibody levels in human cytomegalovirus infection. Sci Transl Med. 2012; 4:128ra42–128ra42.

37. Sibley CG, Comstock JA, Ahlquist JE. DNA hybridization evidence of hominoid phylogeny: a reanalysis of the data. J Mol Evol. 1990; 30:202–236. [PubMed: 2109085]

38. Thiel C, Bontrop RE, Lanchbury JS. Structure and diversity of the T-cell receptor alpha chain in rhesus macaque and chimpanzee. Hum Immunol. 1995; 43:85–94. [PubMed: 7591875]

39. Guo XZJ, et al. Rapid cloning, expression, and functional characterization of paired αβ and γδ T-cell receptor chains from single-cell analysis. Mol Ther Methods Clin Dev. 2016; 3:15054. [PubMed: 26858965]

40. Rhesus Macaque Genome Sequencing and Analysis Consortium. et al. Evolutionary and biomedical insights from the rhesus macaque genome. Science. 2007; 316:222–234. [PubMed: 17431167]

41. Lefranc MP, et al. IMGT, the international ImMunoGeneTics database. Nucleic Acids Res. 1999; 27:209–212. [PubMed: 9847182]

42. Altschul SF, Gish W, Miller W, Myers EW, Lipman DJ. Basic local alignment search tool. J Mol Biol. 1990; 215:403–410. [PubMed: 2231712]

43. Needleman SB, Wunsch CD. A general method applicable to the search for similarities in the amino acid sequence of two proteins. J Mol Biol. 1970; 48:443–453. [PubMed: 5420325]
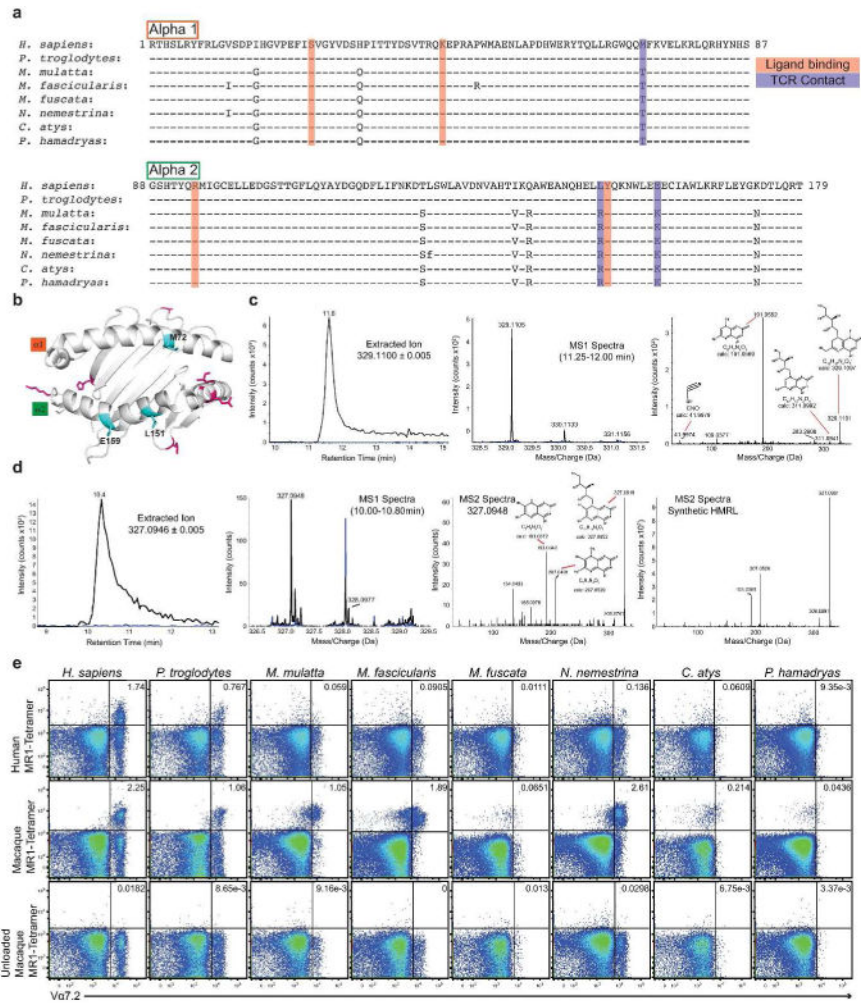
Figure 1. MR1 sequence polymorphisms explain species-specific tetramer reactivity

a) The amino acid alignment of the MR1 α1 and α2 domains is displayed. Identity to the human reference sequence is indicated by a "-". Differences are indicated by the specific amino acid. Lowercase indicates heterozygosity. b) A ribbon diagram of the α1 and α2 domains of the MR1 molecule (from above). TCR contact residues are highlighted in blue. c) Left panel - Negative ion MS1 extracted ion chromatogram of rRL-6-CH2OH ([M-H]⁻ = 329.1100) from macaque MR1 co-cultured with *E. coli* (black) or the macaque MR1 mock control (blue). Middle panel - Composite MS1 spectra from 11.25-12.00 minutes of ion 329.1100. The black trace is macaque MR1 co-cultured with *E. coli* and the macaque MR1 mock control is blue. Right panel - Fragment spectrum of ion 329.1105 at 11.51 minutes from the *E. coli* sample. The precursor and product ions are consistent with the published fragment spectra for synthetic rRL-6-CH2OH. Possible fragment ion structures are shown with their corresponding chemical formula, calculated mass, and observed ion. d) Left Panel - Negative ion MS1 extracted ion chromatogram of HMRL ([M-H]⁻ = 327.0946) from macaque MR1 co-cultured with *E. coli* (black) or the macaque MR1 mock control (blue). Second from left panel - Composite negative ion MS1 spectra from 10.00-10.80 minutes of ion 327.0948. The black trace is macaque MR1 co-cultured with *E. coli* and the macaque

MR1 mock control is blue. Second from right panel - Fragment spectrum of ion 329.0948 at 10.38 minutes from the *E. coli* sample. The precursor and product ions are consistent with the fragment spectra of synthetic HMRL. Possible fragment ion structures are shown with their corresponding chemical formula, calculated mass, and observed ion. Right panel – Fragment spectrum of synthetic HMRL. e) Tetramer staining of PBMC from each of the indicated species is plotted against staining by the anti-Vα7.2 antibody. Plots progressively gated on lymphocytes, singlets, live, CD3+, CD8+ cells.
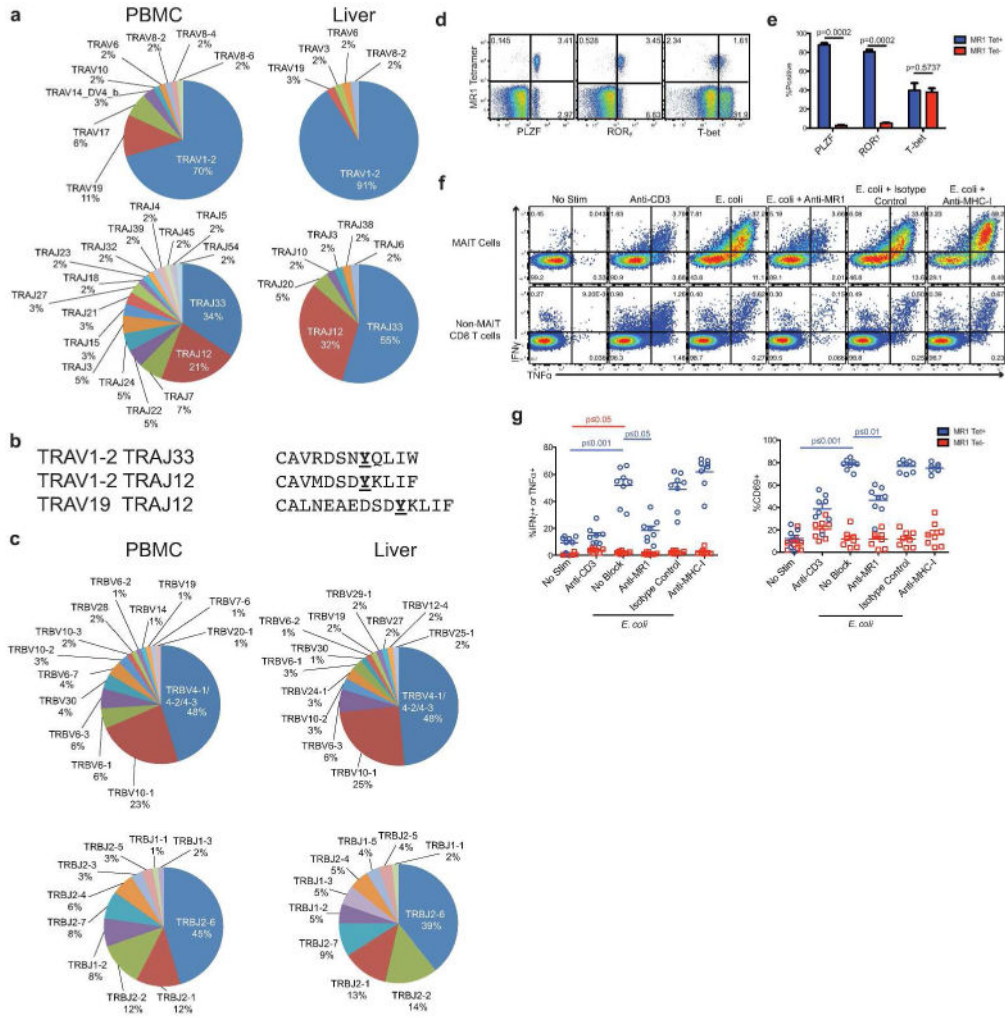
Figure 2. Macaque MR1 tetramer+ cells are phenotypically and functionally similar to human and mouse MAITs

a) TCRαV (top) and J (bottom) region usage from MR1 tetramer+ cells from both the blood (n=61 cells) and liver (n=44 cells) of a healthy macaque. b) Select CDR3α sequences of blood MAITs. The canonical ligand binding tyrosine is noted in bold/underlined. c) TCRβ V (top) and J (bottom) region usage from MR1 tetramer+ cells from blood (n=73 cells) and liver (n=64 cells). TRBV4-1, 4-2 and 4-3 were combined together since they are indistinguishable based on the sequence length of the single cell product. d) Representative nuclear staining for PLZF, RORγ, and T-bet. Plots were progressively gated on lymphocytes, singlets, live, CD3+, and CD8+ cells. e) PBMC from eight animals were stained for the nuclear proteins PLZF, RORγ, and T-bet. Mean, s.e.m. and p values (Wilcoxon Rank Sum test) are shown. f) Representative staining of MAITs (top) and non-MAIT CD8+ T cells (bottom) in a functional assay. g) Functional assay results examining activation of MAITs from spleen of eight animals to PFA fixed *E. coli*. Cells were stained with IFNγ and TNFα (left) and CD69 (right). Results from MR1 tetramer positive cells are shown in blue and MR1 tetramer negative cells in red. All blocking antibodies were added at
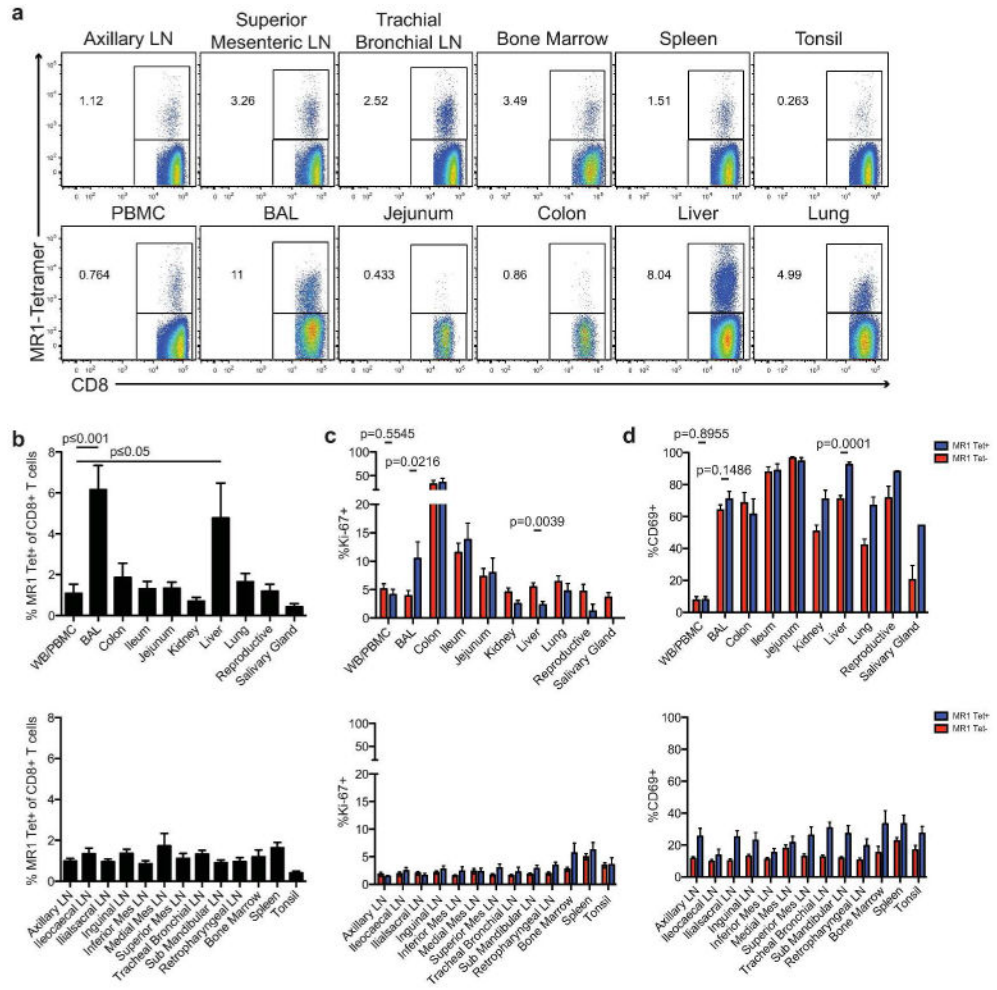
a concentration of 100μg/ml. Conditions were plated in duplicate and averaged. Mean, s.e.m. and p values (Kruskal Wallis and Dunn's Multiple comparison post-test) are shown.

Figure 3. MAIT frequency and phenotype in macaque tissues

a) Representative tetramer staining of multiple macaque tissues. Plots gated on lymphocytes by FSC and SSC, singlets, live, CD3+, CD8+ cells. b) MAIT frequencies among extralymphoid tissues (top) and primary/secondary lymphoid tissues (bottom). 11 animals were stained except for colon which utilized 19 animals and samples were only included if there were at least 300 CD8+ T cells from which to gate tetramer+ cells. Mean, s.e.m. and p values (Kruskal Wallis test followed by Dunn's Multiple Comparison post test) are shown. c) Frequency of Ki-67+ MAITs (blue) and non-MAIT CD8+ T cells (red) in the extralymphoid (top) and primary/secondary lymphoid tissues (bottom). d) Frequency of CD69+ MAITs (blue) and non-MAIT CD8+ T cells (red) in the extralymphoid (top) and primary / secondary lymphoid tissues (bottom). Samples were included in the Ki-67 or CD69 analysis if there were at least 300 CD8+ T cells and at least 10 MR1 tetramer+ cells. Mean, s.e.m. and p values (Wilcoxon Rank Sum test) are shown.
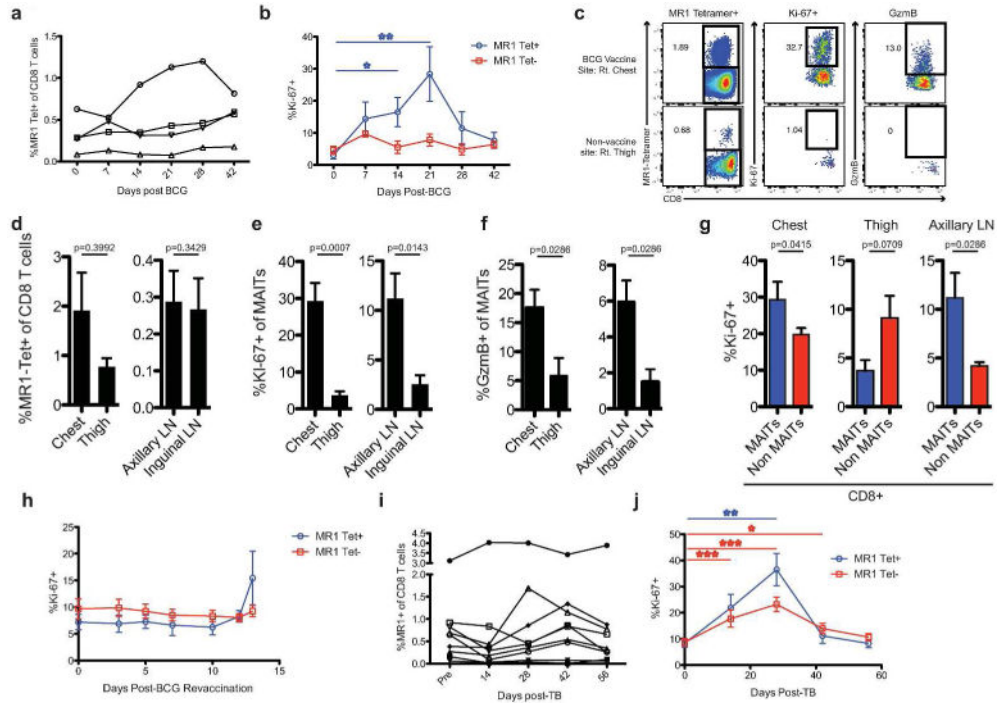
Figure 4. MAITs respond to bacterial pathogens *in vivo*

Four macaques were challenged with BCG intradermally and monitored for 6 weeks. a) Frequency of MAITs in the blood of BCG vaccinated macaques. Mean and s.e.m. are shown. Kruskal Wallis test revealed no significant differences in MAIT frequencies. b) Frequency of Ki-67+ MAITs (blue) and non-MAIT CD8+ T cells (red) in the blood. Mean, s.e.m and p values (Friedman test with Dunn's Multiple comparison post test) are shown (*, p 0.05, **, p 0.01). Animals were revaccinated with BCG 9-weeks post-initial vaccination. These animals were brought to necropsy at days 13 and 14 for analysis. c) Representative MR1-tetramer, Ki-67, and GzmB staining from the pectoral (top, vaccine site) and inguinal (bottom, non-vaccine site) skin sections. d) Frequency of MAITs of CD8+ T cells in the chest and thigh skin sections (left) and in the axillary and inguinal lymph nodes (right). e) Percentage of Ki-67+ MAITs in the chest and thigh sections (left) and axillary and inguinal lymph nodes (right). f) Frequency of GzmB+ MAITs in the skin (left) and lymph nodes (right). g) Comparison of Ki-67+ frequencies among MAITs and non-MAIT CD8+ T cells in the chest (left), thigh (middle), and axillary lymph node (right). Mean, s.e.m. and p values (Wilcoxon Rank Sum test) are shown for parts d-g. h) Ki-67+ frequency of MAITs (blue) and not MAITs (red) after re-vaccination. i) MAIT frequencies of CD8+ T cells in blood after TB infection. j) MAIT and non-MAIT CD8+ T cell Ki-67 frequencies after Mtb infection. Mean, s.e.m and p values (Friedman test with Dunn's Multiple comparison post test) are shown (*, p 0.05; **, p 0.01; ***, p 0.001).